Published in final edited form as:
NMR Biomed. 2006 April ; 19(2): 209–216. doi:10.1002/nbm.1019.

Quantitative glutamate spectroscopic imaging of the human hippocampus

J. W. Pan[1,*], **T. Venkatraman**[1], **K. Vives**[2], and **D. D. Spencer**[2]

[1]Magnetic Resonance Research Center and Department of Neurology, Albert Einstein College of Medicine, Bronx, New York, USA

[2]Department of Neurosurgery, Yale University School of Medicine, New Haven, Connecticut, USA

Abstract

We have evaluated a three-dimensional localized spectroscopic imaging sequence that uses two pairs of adiabatic full-passage pulses, which optimizes the detection of glutamate resonances at moderate echo times. This sequence provides excellent volume localization while simultaneously reducing *J*-modulation losses of glutamate. We have simulated the performance of this sequence for glutamate and used it to quantitatively measure glutamate in the human hippocampus using a linear components model. Using tissue segmentation and regression analysis, we measured a glutamate concentration of 8.8 ± 2.1 mM in hippocampal and temporal gray matter and 3.7 ± 1.1 mM in temporal white matter (95% CI). We have used this approach in a small group of patients (n = 5) with unilateral hippocampal epilepsy.

Keywords

glutamate; spectroscopic imaging; adiabatic; hippocampus

Introduction

In order to minimize *J*-modulation losses, the major approach to the measurement of glutamate and the amino acids remains short echo time spectroscopy (1–3). While this may be adequate for regions of the brain with homogeneous B_0, in the hippocampus the large susceptibility gradients due to adjacent structures including the petrous bone, clivus and sinuses makes short echo time spectroscopy challenging. This region is, however, an important radiographic target because of its participation in numerous diseases. At high field where the greater chemical shift dispersion improves the detection of the amino acids the challenges due to B_0 field inhomogeneity can be severe. Nonetheless, as demonstrated by Capizzano *et al*. and Chu *et al*. (4, 5), successful spectroscopic imaging in the hippocampal region is possible. These studies used longer echo times, which allow for better suppression of water and lipid through relaxation losses and application of more effective gradient crushing. On the other hand, since moderate and longer echo time spectroscopy suffer from signal loss due to increasing *J*-modulation, it is also clear that an approach that can reduce *J*-modulation would be of utility, for single voxel spectroscopy and particularly spectroscopic imaging where the inter-voxel consistency of shimming may be less well controlled.

[*]Correspondence to: J.W. Pan, Magnetic Resonance Research Center, and Department of Neurology, Albert Einstein College of Medicine, Bronx, NY, 10461, USA. jpan@aecom.yu.edu.

In a multi-echo sequence, pairs of adiabatic full passage (AFP) pulses refocus magnetization in a manner that compensates for off-resonance effects and B_1 inhomogeneity (6–8). The LASER (localization by adiabatic selective refocusing) sequence, which uses three pairs of AFP pulses to achieve localization, takes advantage of this feature, as discussed by Garwood and DelaBarre (7). Beyond this effect, however, given the adiabatic nature of the pulse in which the magnetization vector tracks with the B_{eff} sweep and the success of adiabatic heteronuclear decoupling (9), the LASER sequence may be anticipated to suppress homonuclcar *J*-modulation. As stated, this effect should be very helpful in the detection of amino acids, and thus in this report we evaluate a two-dimensional version of the LASER sequence with simulations and phantom measurements. *In vivo* we have implemented this two-dimensional LASER sequence to measure hippocampal glutamate levels in healthy human brain (n = 10 volunteers) using 1.44 cm^3 voxels. In controls, a regression analysis on hippocampal and temporal lobe glutamate with regards to tissue type yielded values consistent with autopsy and biopsy literature (10, 11) in gray and white matter.

Experimental

Sequence: simulation and phantom

The two-dimensional LASER sequence (Fig. 1) uses two pairs of AFP pulses (which can be slice-selective). Water suppression is achieved by a semi-selective excitation pulse (1, 12) in addition to a CHESS water suppression pulse (13).

To simulate this sequence's effects on the glutamate spin system, glutamatc was modeled as a 5 spin $I_aI_bS_aS_bX$ spin system using a density operator simulation [GAMMA, 'General approach to magnetic resonance mathematical analysis' (14)]. Figure 2(a) shows the simulation performed at 4T, demonstrating the retention of glutamate resonances using the two-dimensional LASER sequence over a range of *TEs* as compared with a conventional double echo sequence using two refocusing block pulses. The simulation used hyperbolic secant pulses of three time constants, μ = 10 (15), and was 4.8 ms in duration, $\gamma B_1/2\pi$ strength 1450 Hz. There was little sensitivity to duration of the AFP pulses (t_{AFP} = 19.2 ms, or 4 × 4.8 ms), with the signal retention of glutamatc in the two-dimensional LASER sequence of duration *TE* being similar to that acquired with a double echo sequence of echo time (*TE*)—t_{AFP} [Fig 2(a); compare 18 ms conventional double spin echo with 37.5 ms two-dimensional LASER spin echo of which 19.2 ms is in AFP pulses]. The retention of the glutamate resonance was also simulated with non-optimal B_1, demonstrating more than 95% retention between 60 and 140% of the optimum B_1 (870 up to 2030 Hz).

At 4T, the performance of the two-dimensional LASER sequence was verified in a phantom (10mM acetate, 10 mM creatine and 10mM glutamate), and is shown in Fig. 2(b). The sequence was implemented with two pairs of hyperbolic secant AFP pulses ($\gamma B_1/2\pi$ 1500Hz) with one dimension of ISIS to select an 8 cm^3 voxel, *TR* 2 s, a total echo time of 37.5 ms. In comparison, the double spin echo was implemented using two Shinnar-LeRoux numerically optimized refocusing pulses [duration, 6.4ms, $\gamma B_1/2\pi$1500 Hz (16)]. The performance of this sequence was also simulated for 1.5T. Because of the stronger coupling between the C3, C4 protons, there is a smaller effect in the suppression of *J*-modulation, with the two-dimensional LASER approach being advantageous starting at a total echo time of 40 ms.

In vivo acquisition

All human studies were performed using a Varian 4 T Inova whole body MR system with a transverse electromagnetic (TEM) (17)^{1}H volume head coil. Scout images were acquired with an inversion recovery gradient echo sequence (*TR*/*TIR*/*TE* 2500/850/16). The hippocampal slice was prescribed from an off-midline sagittal slice through the temporal

lobe and defined along the planum temporale. Localized automatic shimming was performed based on a B_0 map using first, second and third order shim corrections (18).

Similar to the phantom acquisition, volume localization (slice 1 cm and anterior—posterior 6 cm) was achieved using two pairs of slice selective AFP pulses (gradients applied on orthogonal axes) and one-dimensional ISIS (8 cm left–right direction). Two-dimensional spectroscopic imaging was superimposed (16 × 16, FOV 19.2 × 19.2 cm^2) to give a nominal voxel size of 1.44 cm^3. An additional non-selective inversion pulse and recovery delay (150 ms) was employed to minimize the macromolecule resonances. The total echo time was 37.5 ms, *TR* 2 s, two averages, resulting in an acquisition time of 34 min. The deposited RF power was within FDA guidelines of 3 W/kg.

Voxel and spectral analysis

The spectroscopic imaging data were processed with a spatial cosine filter and filtered in the time domain with a Lorentz-to-Gauss conversion (2–5 Hz) and a convolution difference for resolution enhancement (50 Hz, weighting 1.0) (19, 20). No other post-acquisition eddy current corrections or water suppression were used. Spectra were selected for analysis with two methods, first for consistent positioning in the hippocampal region, and second for voxels including the hippocampus and temporal lobe. For the former analysis, the scout images were used to semi-automatically position the four (or five) desired loci [Fig. 3(a)]. This positioning was performed after manual definition of the lateral and medial edges of the hippocampi. For each side, the midline of the hippocampus was calculated and five voxel positions (anterior to posterior) were then centered on the midline, each voxel separated by 13.5 mm. The centers of left and right voxel 3 were placed at the level of the midbrain aqueduct. Notably, with the 1.44 cm^3 voxel sizes, hippocampal tissue is largely contained within voxels 2–4. Voxel reconstruction was performed after spatially shifting the spectroscopic imaging data (21). For the latter analysis, which included voxels from the temporal lobe, the spectroscopic imaging grid was used without any spatial shifting to generate a range of gray and white matter.

To analyze the spectral data, locally written software (MATLAB, Natick, MA, USA) based on a linear components model over the spectral range of 1.9–3.4 ppm, was used (22). Six compounds were included: NAA, creatine, glutamate, glutamine, aspartate and choline. The basis set for the model was determined using phantom data (50 m_M concentration) from these compounds. Spectral fits on glutamate demonstrating more than 20% variation in the normalized confidence interval (determined from the residual and Jacobian of the least squares solution) were rejected.

Ratio data are reported relative to NAA since the concentration of NAA has been demonstrated to have a relatively small dependence on gray or white matter distribution (23, 24). Quantification in m_M units was performed by referencing the metabolite area to the CSF water signal obtained from the ambient cistern acquired from a gradient echo proton density image (*TR* 2 s, $\theta = 27$, *TE* 9.3 ms, 128 × 128), The conversion factor, of imaging amplitude into spectral metabolite area, was obtained by the acquisition of a non-water suppressed CSI (using equivalent spectral parameters) taken through the cistern, comparing the integrated water area with imaging signal amplitude. Since the ambient cistern is relatively free of vascular artifacts and the proton density image was acquired after shimming, this provides an excellent reference. At high field, this approach of using an internal reference also decreases errors from differences in B_1 variation that may be present between the *in vivo* brain and phantoms. Tissue volume corrections were made based on quantitative T_1 tissue segmentation as has been previously reported (25). Gray matter fraction was determined as GM/(GM + WM). Relaxation corrections used T_1 and T_2 values for NAA and creatine as previously reported at 4 T (26): T_1 NAA, 1.27 s; T_1 creatine, 1.49 s; T_1 choline, 1.30s; T_2

NAA 230ms; T_2 creatine, I40ms; T_2 choline, 189 ms. While there is no available data on the relaxation time of glutamate in *in vivo* human brain at high field, we would think that creatine in human brain may be a reasonable estimate having the shortest T_2 of the signlet resonances. However, it may be considered that methylene protons can have substantially shorter T_2 relaxation times compared with methyls (shorter by ~40%) (39), which, given the 37 ms echo time, may increase the concentration of glutamate by ~12%. As is evident, errors in relaxation time will contribute to quantitation errors, although the moderate echo time used in these studies limits the effect of T_2 error. Also, as discussed by Michacli *et al.* (27), the T_2 relaxation times of this multispin echo sequence are effectively lengthened (NAA by a factor of 1.68, and creatine 1.8) compared with a single spin echo due to the suppression of diffusion. These relaxation corrections were included in the quantification, using the creatine correction for the amino acids.

$N = 10$ healthy adult subjects were studied (age 30 ± 9, range 18–46, no significant difference between the women and men, five women). For the specific hippocampal data, all subjects had eight spectra analyzed; for the temporal gray/white data, the mean number of pixels analyzed per subject was 12.9 ± 2.4 pixels (range, 9–16). All the patient studies were acquired from unilateral hippocampal epilepsy patients as determined by other clinical data including EEG and MRI data. The mean age of these patients was 30 ± 5years (range 23–36, two women, Table 1). All human studies were performed under IRB approved guidelines.

Results

Figure 3(a) displays a scout image and spectra from the hippocampi of a control volunteer. The spectra shown have no baseline correction. As can be seen, excellent spectra arc obtained bilaterally, posteriorly and anteriorly. Although the use of the inversion recovery pulse and delay docs reduce the available SNR, this approach eliminates the need for a separate macromolecular acquisition and provides a flat baseline for robust analysis. The SNR of glutamate and NAA from locus 3 [Fig. 3(a)] was ~12 and 50 respectively. All of the spectra from the control subjects, loci 1–4 showed a variation in the glutamate concentration of less than 20% and were therefore included in the analysis, Locus 5, located immediately adjacent to the anterior large voxel edge, was not analyzed. Table 2 shows the ratios of glutamate:NAA, Cr:NAA and quantified glutamate, NAA and Cr concentrations across loci 1–4, shown in Fig. 3, In these data, left and right values were not significantly different and were therefore averaged together.

Based on previous data (28, 29), we anticipated that the concentrations of glutamate should vary depending on gray matter content of the voxel. To evaluate this issue we analyzed a wider set of data including both hippocampal, temporal gray and white matter adjacent to the hippocampi to generate a linear regression of glutamate:NAA against fraction gray matter, $R = +0.48$, p 0.001 [Fig. 3(b) shows data from all $n = 10$ volunteers and also shows highlighted data from a single volunteer]. To get an estimate of how consistent the regressions were individually, the mean R-value was determined at 0.63 ± 0.19. The predicted pure white and gray matter ratios of glutamate:NAA are 0.29 ± 0.09 (95% CI) and 0.87 ± 0.18 (95% CI) respectively. Correlation of glutamate concentrations against gray matter directly gave $R = +0.38$, p 0.001 [Fig. 3(c)], while NAA demonstrated a small negative correlation with gray matter content ($R = -0.25$, p 0.005). The concentrations of glutamate in white and gray matter were projected at 3.7 ± 1.1 and 8.8 ± 2.1m_M, respectively. As expected, Cr/NAA also demonstrated a significant correlation with gray matter at $R = +0.33$, p 0.001 (data not shown).

Figure 4 shows spectral data acquired from a patient with temporal lobe epilepsy. The data acquired from the epilepsy patients ($n = 5$) are summarized in Table 3. These patients

showed a significantly higher Cr:NAA, and lower NAA and glutamate concentrations from locus 3 of the ipsilateral hippocampus. Creatine concentrations were not significantly different between control and patient groups.

Discussion

The two-dimensional LASER sequence effectively provides homonuclear decoupling to minimize *J*-modulation losses simultaneously with excellent localization and B_1 insensitivity. This allows the use of longer echo times, which in turn provides for improved water suppression and decreases contributions from macro-molecular resonances, which substantively overlap the amino acid resonances.

Previously we reported the use of a *J*-refocused coherence transfer approach to measure glutamate in the *in vivo* human brain (29). This earlier approach utilized a phase sensitive transfer pulse which resulted in variable transfer efficiencies depending upon B_1 homogeneity and gradient performance, which could not be simultaneously compensated for from all loci in a spectroscopic imaging study. Furthermore, the method required careful phase optimization, lengthening the duration of the study. The present approach provides effective reduction of *J*-modulation that is relatively independent of B_1 homogeneity and gradient performance. Measurement of glutamate is therefore much more consistent across the imaging plane.

The quantified data arc in the same range as previously reported values of NAA, creatine and ratios (30–33) measured in the hippocampus. We have determined that, in healthy brain, the temporal lobe and hippocampus, white matter glutamate:NAA is less than half that seen in gray matter. The quantitative analysis shows that this tissue type sensitivity is primarily a result of the varying levels of glutamate (rather than NAA), showing glutamate at 3.7 ± 1.1 mM (white), 8.8 ± 2.1 mM (gray). The available human brain extract data have considerable variability, depending on method, biopsy vs autopsy, and tissue types (glutamate levels varying from 6 to 10 mM) (10, 11), but are consistent with our measurements. Considering existing MR spectroscopic reports of hippocampal glutamate at high field, Schubert *et al.* (34) used single voxel PRESS at 3 T to report NAA levels of ~11 mM, similar to the present data; however higher glutamate levels at 10.5 mM. Notably, Schubert *et al.* also used multiple quantum filtering to evaluate hippocampal glutamate, finding 8 mM levels, which is in more agreement with the present data. These data are also in agreement with that of Kassem *et al.* (35), who also used single voxel spectroscopy (1.7 cm^3) at 4T to report ~8 mM glutamate in the posterior hippocampus (similar to loci 2–3 of Table 2).

As expected, the epilepsy patients showed a decline in NAA:Cr in the ipsilateral hippocampus. Quantification relative to ambient cistern CSF and correction for tissue volume demonstrated that the decline occurs in NAA rather than any large increase in creatine, consistent with literature data (36). Given the decline in ipsilateral hippocampal NAA, the epilepsy patients did not show any difference in glutamale:NAA ipsilaterally compared with controls. In this small group the decline in glutamate appears to parallel that of NAA, with ipsilaleral glutamate and NAA al 4.2 ± 1.3 and 7.1 ± 0.7 mM compared with 6.0 ± 1.3 and 8.9 ± 0.9 mM in controls respectively, yielding declines of approximately 30% in glutamate and 20% in NAA. Notably, the present data show a more than doubling of glutamate content between white and gray matter, emphasizing the importance of tissue content determinations. For example, *a priori*, it is possible that the decreased glutamate concentration in these patients is due to a decline in fractional gray matter. However in these patients, the fraction gray matter from locus 3 was comparable to that of controls (contralateral hippocampus, 51.8 ± 6.3%; ipsilaleral hippocampus 47.4 ± 7.3%; control 47.6 ± 5.3%).

We may compare these data to other studies of glutamate in temporal lobe epilepsy. Simister *et al.* (37) used short echo time spectroscopic imaging at 1.5 T to study $n = 20$ temporal lobe epilepsy patients (10 with normal hippocampi; 10 with hippocampal sclerosis) in comparison to control, finding that while the glutamate + glutamine (Glx) level was elevated in the group with normal hippocampi compared with control, the 10 patients with hippocampal sclerosis had similar levels in Glx content lo control volunteers. This latter comparison is closest to the present group of patients, in which Tour out of live patients demonstrate lateralized abnormalities in structural MR imaging ('MRI positive' group, showing hipppocampal atrophy and signal change, typical of hippocampal sclerosis, Table 1). The observation of larger Glx at 1.5 T may arise from the contribution of glutamate, glutamine and possibly macromolecules to the Glx resonance, From the present data, and the known role of glutamate as a key compound in intermediary metabolism, it may not be surprising that we find declines in glutamate concentrations that parallel NAA, a measure of mitochondrial function (38). However, what is of interest is the level of hippocampal glutamate in the 'MRI negative' (those TLE patients with normal hippocampi), as it is possible that elevated glutamate levels contribute to hyperexcitability, as suggested by Simister *et al.* (37).

By virtue of the suppression of *J*-modulation, the modified two-dimensional LASER sequence allows the excellent detection of glutamate at relatively longer echo times. The sequence has minimal need for peak power and gradient optimization. We have quantitatively implemented this approach in the healthy human hippocampus, reporting metabolite concentrations that are within reported autopsy and biopsy values.

References

1. Pouwels PJ, Frahm J. Regional metabolite concentrations in human brain as determined by quantitative localized proton MRS. Magn Reson Med. 1998; 39(1):53–60. [PubMed: 9438437]
2. Soher BJ, Vermathen P, Schuff N, Wiedermann D, Meyerhoff DJ, Weiner MW, Maudsley AA. Short *TE in vivo* (1)H MR spectroscopic imaging at 1.5 T: acquisition and automated spectral analysis. Magn Ream Imag. 2000; 18(9):1159–1165.
3. Zhong K, Ernst T. Localized *in vivo* human ^{1}H MRS at very short echo times. Magn Reson Med. 2004; 52(4):898–901. [PubMed: 15389966]
4. Capizzano AA, Vermathen P, Laxcr KD, Matson GB, Maudsley AA, Sohcr BJ, Schuff NW, Weiner MW. Multisection proton MR spectroscopy for mesial temporal lobe epilepsy. AJNR Am J Neuroradiol. 2002; 23(8):1359–1368. [PubMed: 12223379]
5. Chu WJ, Kuzniecky RI, Hugg JW, Abou-Khalil B, Gilliam F, Faught E, Hetherington HP. Statistically driven identification of focal metabolic abnormalities in temporal lobe epilepsy with corrections for tissue heterogeneity using ^{1}H spectroscopic imaging. Magn Ream Med. 2000; 43(3): 359–367.
6. Conolly S, Glover G, Nishimura D, Macovski A. A reduced power selective adiabatic spin-echo pulse sequence. Magn Reson Med. 1991; 18(1):28–38. [PubMed: 2062239]
7. Garwood M, DelaBarre L. The return of the frequency sweep: designing adiabalic pulses for contemporary NMR. J Magn Reson. 2001; 153(2):155–177. [PubMed: 11740891]
8. de Graaf RA, Luo Y, Garwood M, Nicolay K. B_1-insensitive, single-shot localization and water suppression. J Magn Reson B. 1996; 113(1):35–45. [PubMed: 8888589]
9. Starcuk Z, Bartusek K, Starcuk Z. Heteronuclear broadband spin flip decoupling with adiabatic pulses. J Magn Reson A. 1994; 107:24–31.
10. Perry TL, Hansen S, Berry K, Mok C, Lesk D. Free amino acids and related compounds in biopsies or human brain. J Neurochem. 1971; 18(3):521–528. [PubMed: 5559258]
11. Lavoie J, Giguere J, Layrargues GP, Butterworth RF. Amino acid changes in autopsied brain tissue from cirrhotic patients with hepatic encephalopathy. J Neurochem. 1987; 49:692–697. [PubMed: 2886551]

12. Hore PJ. Nuclear magnetic resonance. Solvent suppression. Meth Enzymol. 1989; 176:64–77. [PubMed: 2811699]
13. Frahm J, Bruhn H, Gyngell M, Merholdt K, Hanicke W, Sauter R. Localized high resolution ^{1}H MR spectroscopy using stimulated echoes: initial applications to human brain *in vivo*. Mugn Reson Med. 1989; 9:79–93.
14. Smith SA, Levante TO, Meier BH, Ernst RR. Computer simulations in magnetic resonance: an object oriented programming approach. J Magn Reson. 1994; 106A:75–105.
15. Silver MS, Joseph RI, Hoult DI. Highly selective/2 and pulse generation. J Magn Reson. 1984; 59:347–351.
16. Matson GB. An integrated program for amplitude-modulated RF pulse generation and re-mapping with shaped gradients. Magn Reson Imag. 1994; 12(8):1205–1225.
17. Vaughan JT, Hetherington HP, Otu JO, Pan JW, Noa PJ, Pohost GM. High frequency volume coils for clinical NMR imaging and spectroscopy. Magn Reson Med. 1994; 32:206–218. [PubMed: 7968443]
18. Hetherington, H.; Pan, J. Proc Int Soc Magnetic Resonance Medicine. Miami Beach, FL: 2005. An automated shim mapping method for spectroscopic imaging of the human hippocampus; p. 730
19. Mazzco AR, Levy GC. An evaluation of new processing protocols for *in vivo* NMR spectroscopy. Magn Reson Med. 1991; 17:483–495. [PubMed: 1648161]
20. Ernst, RR. Advances in Magnetic Resonance. Waugh, JS., editor. Academic Press; New York: 1966. p. 1-135.
21. Twieg DB, Meyerhoff D, Hubesch B, Roth K, Sappey-Marinier D, Boska MD, Cober JR, Schaefer S, Weiner MW. P^{31} MR spectroscopy in humans by spectroscopic imaging: localized spectroscopy and metabolite imaging. Magn Reson Med. 1989; 12:291–305. [PubMed: 2628680]
22. Provencher SW. Automatic quantitation of localized *in vivo* ^{1}H spectra with LCModel. NMR Biomed. 2001; 14(4):260–264. [PubMed: 11410943]
23. Tedeschi G, Righini A, Bizzi A, Barnett AS, Alger JR. Cerebral white matter in the centrum semiovale exhibits a larger *N*-acctyl signal than docs gray matter in long echo time H-magnetic resonance spectroscopic imaging. Magn Reson Med. 1995; 33(1):127–133. [PubMed: 7891527]
24. Schuff N, Ezekiel F, Gamst AC, Amend DL, Capizzano AA, Maudsley AA, Weiner MW. Region and tissue differences of metabolites in normally aged brain using multislice ^{1}H magnetic resonance spectroscopic imaging. Magn Res Med. 2001; 45(5):899–907.
25. Chu WJ, Kuzniecky RI, Hugg JW, Abou-Khalil B, Gilliam F, Faught E, Hetherington HP. Statistically driven identification of focal metabolic abnormalities in temporal lobe epilepsy with corrections for tissue heterogeneity using ^{1}H spectroscopic imaging. Magn Reson Med. 2000; 43(3):359–367. [PubMed: 10725878]
26. Hetherington HP, Mason GF, Pan JW, Ponder SL, Vaughan JT, Twicg DB, Pohost GM. Evaluation of cerebral gray and white matter metabolite differences by spectroscopic imaging at 4.1 T. Magn Reson Med. 1994; 32(5):565–571. [PubMed: 7808257]
27. Michacli S, Garwood M, Zhu XH, DelaBarrc L, Andersen P, Adriany G, Merkle H, Ugurbil K, Chen W. Proton T_2 relaxation study of water, *N*-acetylaspartate, and creatine in human brain using Hahn and Carr–Purcell spin echoes at 4 T and 7 T. Magn Reson Med. 2002; 47(4):629–633. [PubMed: 11948722]
28. Mason CF, Pan JW, Ponder SL, Twieg DB, Pohost CM, Hetherington HP. Detection of brain glutamate and glutamine in spectroscopic images at 4.1 T. Magn Reson Med. 1994; 32:142–145. [PubMed: 7916115]
29. Pan JW, Mason GF, Pohost GM, Hetherington HP. Spectroscopic imaging of human brain glutamale by water-suppressed J-refocused coherence transfer at 4.1 T. Magn Reson Med. 1996; 36(1):7–12. [PubMed: 8795013]
30. Wellard RM, Briellmann RS, Prichard JW, Syngcniotis A, Jackson GD. *Myo*-inositol abnormalities in temporal lobe epilepsy. Epilepsia. 2003; 44(6):813–821.
31. Jiru F, Dezortova M, Burian M, Hajek M. The role of relaxation time corrections for the evaluation of long and short echo time ^{1}H MR spectra of the hippocampus by NUMAR1S and LCModel techniques. MAGMA. 2003; 16(3):135–143. [PubMed: 14564645]

32. Due CO, Trabesinger AH, Weber OM, Meier D, Walder M, Wieser HG, Boesiger P. Quantitative ^{1}H MRS in the evaluation of mesial temporal lobe epilepsy in vivo. Magn Reson Imag. 1998; 16(8):969–979.
33. Cohen-Gadol AA, Pan JW, Kim JH, Spencer DD, Hemerington HP. Mesial temporal lobe epilepsy: a proton MR spectroscopy study and a histpathological analysis. J Neurosurg. 2004; 101:613–620. [PubMed: 15481715]
34. Schubert F, Gallinat J, Seifert F, Rinneberg H. Glutamate concentrations in human brain using single voxel proton magnetic resonance spectroscopy at 3 Tesla. Neuroimage. 2004; 21(4):1762–1771. [PubMed: 15050596]
35. Kassem MN, Bartha R. Quantitative proton short-echo-time LASER spectroscopy of normal human white matter and hippocampus at 4 Tesla incorporating macromolecule subtraction. Magn Reson Med. 2003; 49(5):918–927. [PubMed: 12704775]
36. Mueller SG, Laxer KD, Suhy J, Lopez RC, Flenniken DL, Weiner MW. Spectroscopic metabolic abnormalities in mTLE with and without MRI evidence for mesial temporal sclerosis using hippocampal short-TE MRSI. Epilepsia. 2003; 44(7):977–980. [PubMed: 12823584]
37. Simisier RJ, Woermann FG, McLean MA, Bartlett PA, Barker GJ, Duncan JS. A short-echo-time proton magnetic resonance spectroscopic imaging study of temporal lobe epilepsy. Epilepsia. 2002; 43:1021–1031. [PubMed: 12199727]
38. Clark IB. *N*-acetyl aspartate: a marker for neuronal loss or mitochondrial dysfunction. Devl Neurosci. 1998; 20(4–5):271–276.
39. Hwang JH, Pan JW, Heydari S, Hetherington HP, Stein DT. Regional differences in intramyocellular lipids in humans observed by *in vivo* ^{1}H-MR spectroscopic imaging. J Appl Physoil. 2001; 90(4):1267–1274.

Abbreviations used

B_0	static magnetic field strength
B_{eff}	effective radiofrequency field strength
BW	bandwidth
CHESS	chemical shift selective
CI	confidence interval
Ch	choline
Cr	creatine
CSF	cerebrospinal fluid
FOV	field of view
Glu	glutamate
ISIS	image selected *in vivo* spectroscopy
LASER	localization by adiabatic selective refocusing
MTS	mesial temporal sclerosis
NAA	*N*-acelyl aspartate
PRESS	point-resolved spectroscopy
R	correlation coefficient
SLR	Shinnur–LeRoux pulse design algorithm
TE	echo time
TR	repetition time

TIR	inversion recovery delay

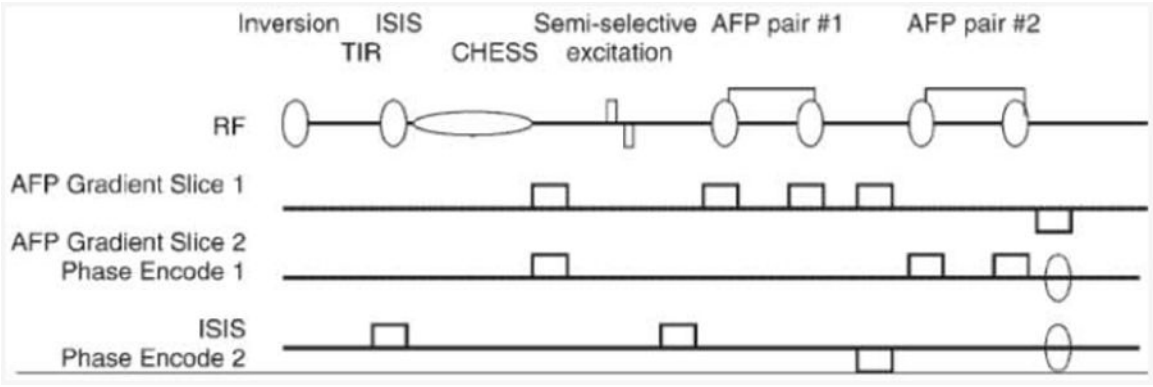

Figure 1.
Pulse sequence, including localization, water suppression and inversion recovery.

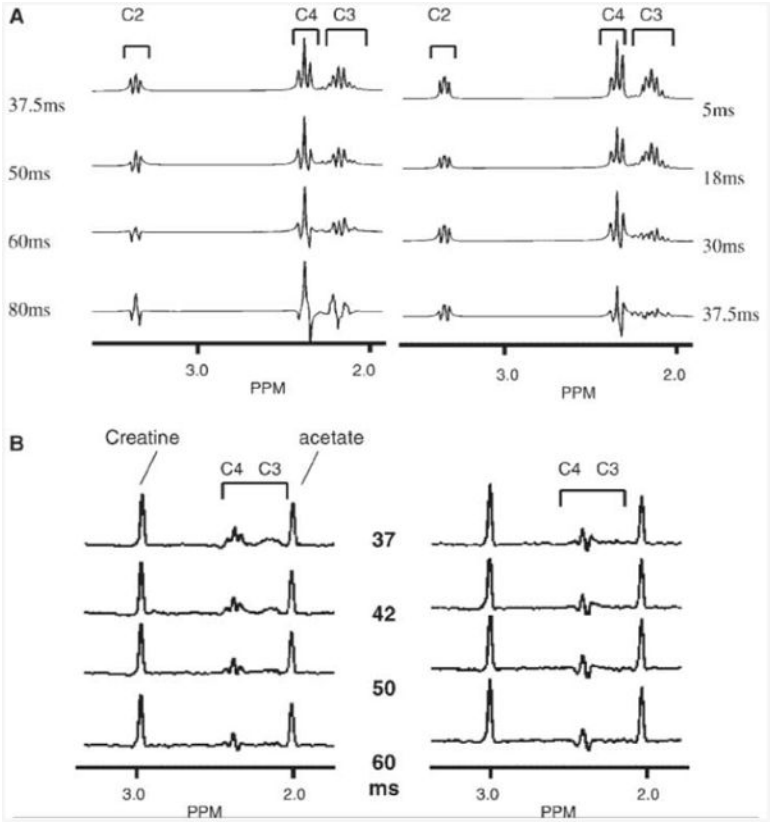

Figure 2.

(A) Simulation of two-dimensional LASER (left) and conventional double echo (right) sequences for glutamate, performed at 4T. (B) Phantom spectra (glutamate, creatine, acetate) showing retention of glutamate resonances, LASER (left), double spin echo (right). Timings are indicated, In both (A) and (B), the brackets indicate the individual glutamate resonances.

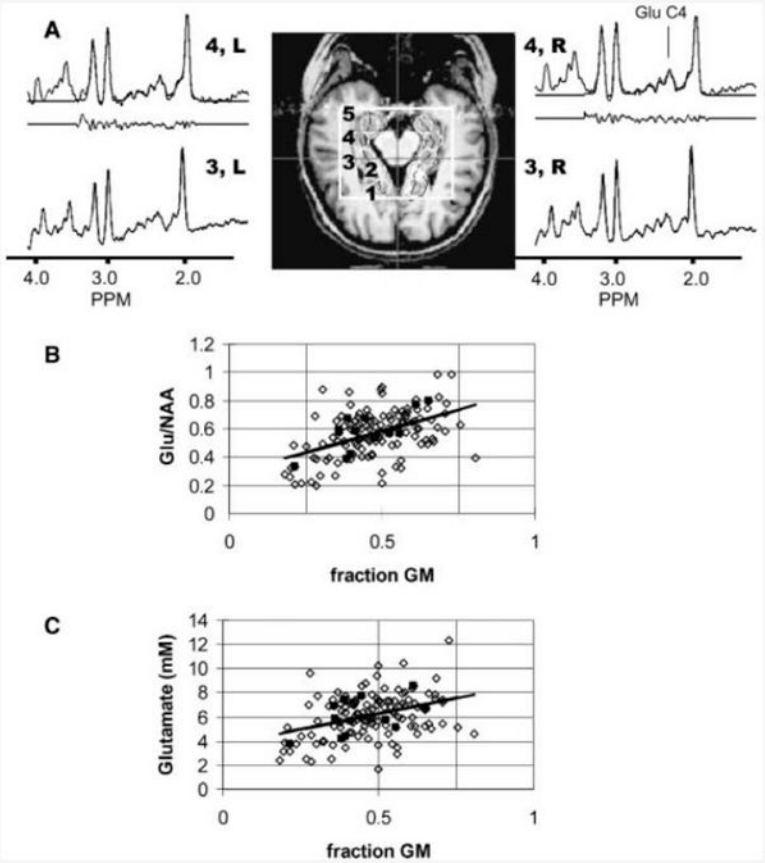

Figure 3.

(A) Hippocampal scout, definition of loci 1–5 (loci *2*–4 including hippocampal tissue) and indicated spectra from a healthy control. The outlined box indicates the large voxel selection. The loci were consistently determined after manual definition of the midbrain aqueduct (indicated by crosshairs) and the hippocampi. For the loci 4L and 4R, the spectral analysis is shown with the fitted, original spectra and residual. The position of glutamate (2.35 ppm) is indicated in the spectra. Regression plots of glutamate:NAA (B) and glutamate concentration (C) with fraction of gray matter from the hippocampal and temporal region. The solid symbols are data from a single volunteer (same volunteer in both ratio and concentration plots).

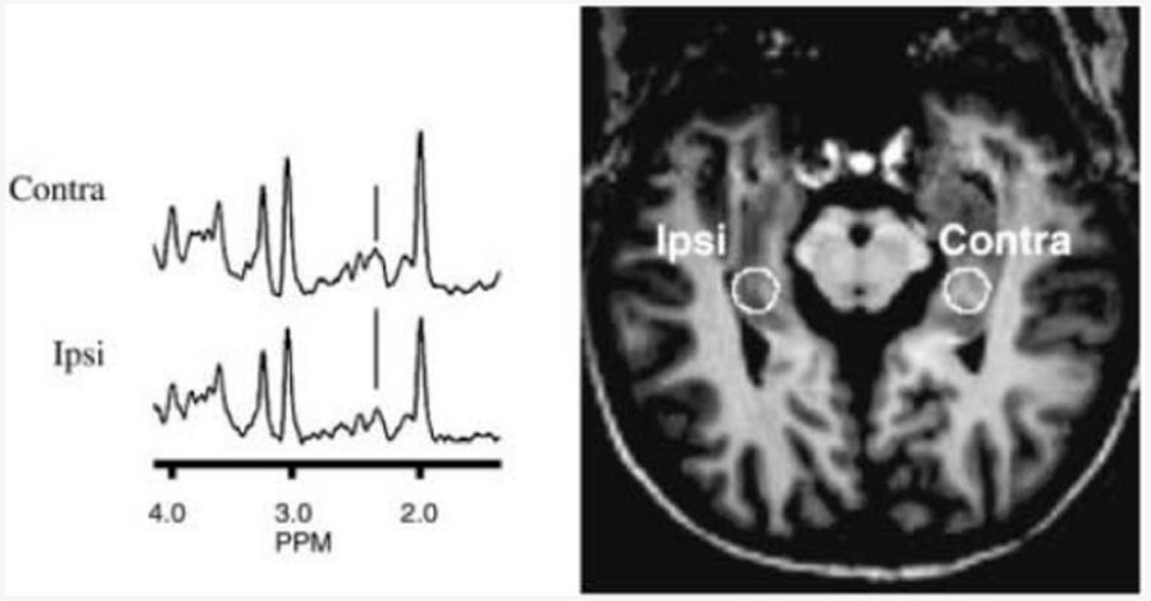

Figure 4.
Hippocampal scout and spectra (locus 3) from a 38-year-old epilepsy patient. The seizure lateralization is indicated on the patient scout image. The position of glutamate (2.35 ppm) is indicated.

Table 1

Epilepsy patients (=5): clinical data

ID	Age	Gender	Handedness	Seizure type	MRI[a]	Outcome
1	23	M	R	R MTS, bilateral	−	Ib
2	36	M	R	R MTS, bilateral	+	Ia
3	34	F	R	R MTS	+	Ia
4	27	M	R	LMTS	+	Ia
5	30	F	R	R MTS, bilateral	+	Ia

[a]MRI: structural imaging data: (−) normal MR1; (+) lateralizing abnormal MRI; MTS: mesial temporal sclerosis. Clinical outcomes Ia, no seizures and no auras; Ib, mild aura only.

NMR Biomed. Author manuscript; available in PMC 2013 May 20.

Table 2

Means and standard deviations for metabolite ratios and concentrations (m_M) in healthy human brain (see Fig. 3 for definition of loci)

	Hippocampus			
	1	**2**	**3**	**4**
Cr:NAA	0.79 ± 0.11	0.85 ± 0.06	0.89 ± 0.06	0.93 ± 0.16
Glutamate:NAA	0.62 ± 0.16	0.69 ± 0.08	0.64 ± 0.11	0.67 ± 0.24
NAA	10.2 ± 1.8	10.5 ± 1.1	8.9 ± 0.9	8.0 ± 1.8
Glutamate	6.7 ± 2.2	7.7 ± 1.3	6.0 ± 1.3	5.4 ± 1.7
Creatine	8.8 ± 1.6	9.9 ± 1.2	8.7 ± 1.0	8.4 ± 2.1
Choline	2.5 ± 0.5	3.9 ± 0.5	3.7 ± 0.6	3.5 ± 0.8
Percentage gray matter	62 ± 7	54 ± 5	48 ± 5	61 ± 5
Percentage CSF	21 ± 5	18 ± 6	7 ± 4	8 ± 3

Table 3

Control (=10) and epilepsy patients (=5), evaluating locus 3, with means and standard deviations for metabolite ratios and concentrations (m_M)

	Control	Ipsi	Contra
Cr:NAA	0.89 ± 0.06	1.08 ± 0.08[a]	0.98 ± 0.09[a]
Gluiamale:NAA	0.64 ± 0.11	0.56 ± 0.10	0.58 ± 0.13
NAA	8.9 ± 0.9	7.1 ± 0.7[a]	8.5 ± 1.2
Glutamate	6.0 ± 1.3	4.2 ± 1.3[a]	5.3 ± 1.8
Creatine	8.7 ± 1.0	8.5 ± 1.3	9.3 ± 1.9
Choline	3.7 ± 0.6	3.0 ± 0.3	2.7 ± 0.7
Percentage gray matter	48 ± 5	47 ± 7	52 ± 6
Percentage CSF	7 ± 4	9 ± 5	7 ± 5

[a]Significantly different from control, p 0.05.